

Simplifying the complexity of pipe flow

Dwight Barkley*

Mathematics Institute, University of Warwick, Coventry CV4 7AL, United Kingdom
 PMMH (UMR 7636 CNRS - ESPCI - Univ Paris 06 - Univ Paris 07), 10 rue Vauquelin, 75005 Paris France
 (Dated: October 26, 2018)

Transitional pipe flow is modeled as a one-dimensional excitable and bistable medium. Models are presented in two variables, turbulence intensity and mean shear, that evolve according to established properties of transitional turbulence. A continuous model captures the essence of the puff-slug transition as a change from excitability to bistability. A discrete model, that additionally incorporates turbulence locally as a chaotic repeller, reproduces almost all large-scale features of transitional pipe flow. In particular it captures metastable localized puffs, puff splitting, slugs, a continuous transition to sustained turbulence via spatiotemporal intermittency (directed percolation), and a subsequent increase in turbulence fraction towards uniform, featureless turbulence.

PACS numbers: 47.27.Cn, 47.27.ed, 47.27.nf, 47.20.Ft

The transition to turbulence in pipe flow has been the subject of study for over 100 years [1], both because of its fundamental role in fluid mechanics and because of the detrimental consequences of turbulent transition in many practical situations. There are at least two features of the problem that make it fascinating, but also difficult to analyze. The first is that when turbulence appears, it appears abruptly [1], and not through a sequence of transitions each increasing the dynamical complexity of the flow. Turbulence is triggered by finite-sized disturbances to linearly stable laminar flow [2–4]. This hysteretic, or subcritical, aspect of the problem limits the applicability of linear and weakly nonlinear theories. The second complicating feature is the intermittent form turbulence takes in the transitional regime near the minimum Reynolds number (non-dimensional flow rate) for which turbulence is observed [1, 5–7]. In sufficiently long pipes, localized patches of turbulence (puffs) may persist for extremely long times before abruptly reverting to laminar flow [8–15]. In other cases, turbulent patches may spread by contaminating nearby laminar flow (puff splitting and slugs) [6, 7, 16–19]. While minimal models have been very useful in understanding generic features of intermittency in subcritical shear flows [20–24], such models do not capture the puffs, puff splitting, and slugs that are essential to the character of pipe flow. In this paper I argue that transitional pipe flow should be viewed in the context of excitable and bistable media. With this perspective I present models, based on the interaction between turbulence and the mean shear, that both capture and organize most large-scale features of transitional pipe flow.

Figure 1 summarizes the three important dynamical regimes of transitional pipe flow. The left column shows results from direct numerical simulations (DNS) [7, 25]. Quantities are nondimensionalized by the pipe diameter D and the mean (bulk) velocity U . The Reynolds number is $Re = DU/\nu$, where ν is kinematic viscosity. Flows are well represented by two quantities, the turbulence intensity q and the axial (streamwise) velocity u , sampled on the pipe axis. Specifically, q is the magnitude of transverse fluid velocity (scaled up by a factor of 6). The centerline velocity u is relative to

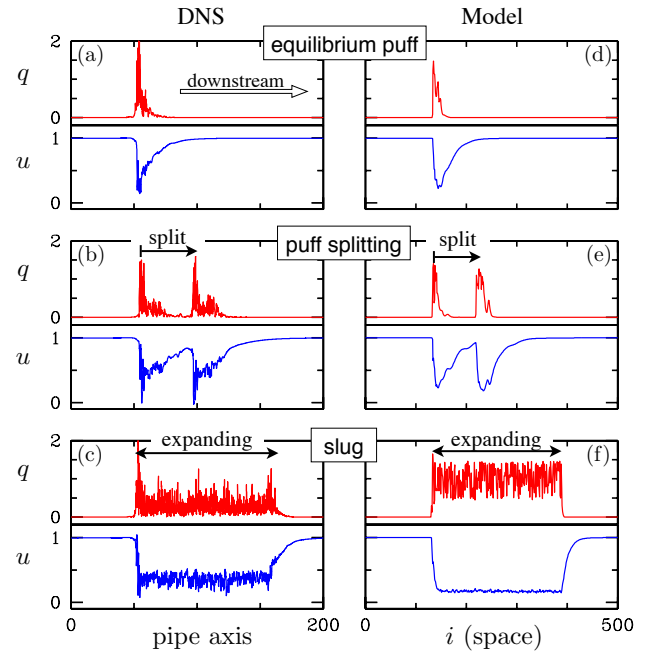


FIG. 1. (Color online) Regimes of transitional pipe flow. Left column is from full DNS with 4×10^7 degrees of freedom in a periodic pipe $200D$ long. Flow is from left to right. Shown are instantaneous values of turbulence intensity q and axial velocity u along the pipe axis. (a) Equilibrium puff at $Re = 2000$. (b) Puff splitting at $Re = 2275$. The downstream (right) puff split from the upstream one at an earlier time. (c) Expanding slug flow at $Re = 3200$. Right column shows corresponding states from the simple one-dimensional model (3)–(6) (d) $R = 2000$, (e) $R = 2100$, and (f) $R = 3200$.

the mean velocity and is a proxy for the state of the mean shear that conveniently lies between 0 and 1. At low Re , as in Fig. 1(a), turbulence occurs in localized patches propagating downstream with nearly constant shape and speed. These are called equilibrium puffs [2, 16, 17], a misnomer since at low Re puffs are only metastable and eventually revert to laminar flow, i.e. decay [8–15]. Asymptotically the flow will be laminar parabolic flow, ($q = 0, u = 1$), throughout the pipe. For intermediate Re , as in Fig. 1(b), puff splitting frequently

* Email: D.Barkley@warwick.ac.uk

occurs [7, 16, 17, 19]. New puffs are spontaneously generated downstream from existing ones and the resulting pairs move downstream with approximately fixed separation. Further splittings will occur and interactions will lead asymptotically to a highly intermittent mixture of turbulent and laminar flow [5, 7]. At yet higher Re , turbulence is no longer confined to localized patches, but spreads aggressively in so-called slug flow [6, 17], as illustrated in Fig. 1(c). The asymptotic state is uniform, featureless turbulence throughout the pipe [7].

Models for these dynamics will be based on the following known physical features. At the upstream (left in Fig. 1) edge of turbulent patches, laminar flow abruptly becomes turbulent. Energy from the laminar shear is rapidly converted into turbulent motion and this results in a rapid change to the mean shear profile [6, 26]. In the case of puffs, the turbulent profile is not able to sustain turbulence and thus there is a reverse transition [6, 27] from turbulent to laminar flow on the downstream side of a puff. In the case of slugs, the turbulent shear profile can sustain turbulence indefinitely; there is no reverse transition and slugs grow to arbitrary streamwise length [6, 17]. On the downstream side of turbulent patches the mean shear profile recovers slowly [27], seen in the behavior of u in Fig. 1. Crucially, the degree of recovery dictates how susceptible the flow is to re-excitation into turbulence [26].

These are the characteristics of excitable and bistable media [28, 29]. In fact the puff in Fig. 1(a) bears a close resemblance to an action potential in a nerve axon [30]. Linearly stable parabolic flow is the excitable rest state, turbulence is the excited state, and the mean shear is the recovery variable controlling the threshold for excitation. Thus, I propose to model pipe flow as a generic excitable and bistable medium incorporating the minimum requisite features of pipe turbulence. The models are expressed in variables q and u depending on distance along the pipe.

Consider first the continuous model

$$\begin{aligned} q_t + Uq_x &= q(u + r - 1 - (r + \delta)(q - 1)^2) + q_{xx}, \quad (1) \\ u_t + Uu_x &= \epsilon_1(1 - u) - \epsilon_2uq - u_x, \quad (2) \end{aligned}$$

where r plays the role of Re . U accounts for downstream advection by the mean velocity, and is otherwise dynamically irrelevant since it can be removed by a change of reference frame. The model includes minimum derivatives, q_{xx} and u_x , needed for turbulent regions to excite adjacent laminar ones and for left-right symmetry breaking.

The core of the model is seen in the q - u phase plane in Fig. 2. The trajectories are organized by the nullclines: curve where $\dot{u} = 0$ and $\dot{q} = 0$ for the local dynamics ($q_{xx} = q_x = u_x = 0$). For all r the nullclines intersect in a stable, but excitable, fixed point corresponding to laminar parabolic flow. The u dynamics with $\epsilon_2 > \epsilon_1$ captures in the simplest way the behavior of the mean shear. In the absence of turbulence ($q = 0$), u relaxes to $u = 1$ at rate ϵ_1 , while in response to turbulence ($q > 0$), u decreases at a faster rate dominated by ϵ_2 . Values $\epsilon_1 = 0.04$ and $\epsilon_2 = 0.2$ give reasonable agreement with pipe flow. (See the Appendix Sec. 1 a.) The q -nullcline consists of $q = 0$ (turbulence is not spontaneously generated from laminar flow) together with a parabolic curve whose nose varies with r , while maintaining a fixed intersec-

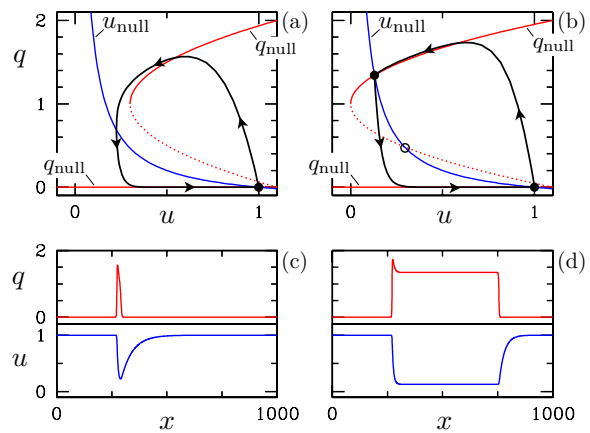


FIG. 2. (Color online) The distinction between puffs and slugs seen as the difference between excitability and bistability in Eqs. (1)-(2). Phase planes show nullclines at (a) $r = 0.7$ and (b) $r = 1$. The fixed point $(1, 0)$ corresponds to parabolic flow. In (b) the additional stable fixed point corresponds to stable turbulence. Solution snapshots show (c) a puff at $r = 0.7$ and (d) a slug at $r = 1$. These solutions are plotted in the phase planes with arrows indicating increasing x .

tion with $q = 0$ at $u = 1 + \delta$, ($\delta = 0.1$ is used here). The upper branch is attractive, while the lower branch is repelling and sets the nonlinear stability threshold for laminar flow. If laminar flow is perturbed beyond the threshold (which decreases with r like r^{-1}), q is nonlinearly amplified and u decreases in response.

The (excitable) puff regime occurs for $r < r_c \simeq \epsilon_2/(\epsilon_1 + \epsilon_2)$, Figs. 2(a) and (c). The upstream side of a puff is a trigger front [28] where abrupt laminar to turbulent transition takes place. However, turbulence cannot be maintained locally following the drop in the mean shear. The system relaminarizes (reverse transition) on the downstream side in a phase front [28] whose speed is set by the upstream front. Following relaminarization, u relaxes and laminar flow regains susceptibility to turbulent perturbations. The slug regime occurs for $r > r_c$, Figs. 2(b) and (d). The nullclines intersect in additional fixed points. The system is bistable and turbulence can be maintained indefinitely in the presence of modified shear. Both the upstream and downstream sides are trigger fronts, moving at different speeds, giving rise to an expansion of turbulence. A full analysis will be presented elsewhere.

While Eqs. (1)-(2) capture the basic properties of puffs and slugs, the turbulence model is too simplistic to show puff decay and puff splitting. Evidence suggests that pipe turbulence is locally a chaotic repeller [31]. Hence a more realistic model, within the two-variable excitability setting, is obtained by replacing the upper turbulent branches in Fig. 2 with a wedged-shaped region of transient chaos, illustrated in Fig. 3. Outside this region q decays monotonically. The model is

$$\begin{aligned} q_{i+1}^{n+1} &= F(q_i^n + d(q_{i-1}^n - 2q_i^n + q_{i+1}^n), u_i^n), \quad (3) \\ u_{i+1}^{n+1} &= u_i^n + \epsilon_1(1 - u_i^n) - \epsilon_2u_i^nq_i^n - c(u_i^n - u_{i-1}^n), \quad (4) \end{aligned}$$

where q_i^n and u_i^n denote values at spatial location i and time n . This model is essentially a discrete version of Eqs. (1)-(2),

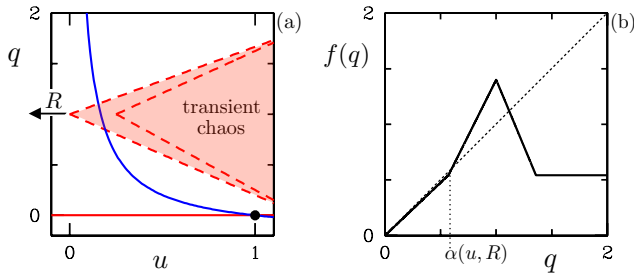


FIG. 3. (Color online) Illustration of the discrete model. (a) Local dynamics in the u - q phase plane. Within a wedge-shaped region q undergoes transient chaos, while outside it decays monotonically to $q = 0$. The region varies with R as indicated. (b) Map used to produce transient chaos. Parameter α (which depends on u and R), is the lower boundary separating monotonic and chaotic dynamics.

except with chaotic q dynamics generated by the map F .

The map F is based on models of chaotic repellers in shear flows [23, 32]. Consider the tent map f given by

$$f(q) = \begin{cases} \gamma q & \text{if } q < Q_1 \\ 2q - \alpha & \text{if } Q_1 \leq q < 1 \\ 4 + \beta - \alpha - (2 + \beta)q & \text{if } 1 \leq q < Q_2 \\ \gamma Q_1 & \text{if } Q_2 \leq q \end{cases} \quad (5)$$

with $Q_1 = \alpha/(2 - \gamma)$ and $Q_2 = (4 + \beta - \alpha - \gamma Q_1)/(2 + \beta)$. Parameter α marks the lower boundary separating chaotic and monotonic dynamics, Fig. 3(b), while γ sets the decay rate to the fixed point $q = 0$. For $\beta > 0$ ($\beta < 0$) the map generates transient (persistent) chaos within the tent region. The map is incorporated into the pipe model by having the threshold α depend on u as well as on a control parameter R , via

$$\alpha = 2000(1 - 0.8u)R^{-1}. \quad (6)$$

The factor $(1 - 0.8u)$ generates the desired wedged-shaped region, while 2000 sets the scale of R to that of Re . Finally, the map F is given by k iterates of f , i.e. $F = f^k$, with $k = 2$ used here. (See the Appendix Sec. 1 b.) This has the effect of increasing the Lyapunov exponent within the chaotic region.

The only important new parameter introduced in the discrete model is β since it quantifies a new effect – spontaneous decay of local turbulence for $\beta > 0$. Suitable values for others are: $\epsilon_1 = 0.04$ and $\epsilon_2 = 0.2$ as before, $\gamma = 0.95$, $c = 0.45$ and $d = 0.15$. (See the Appendix Sec. 1 b.) As shown in Fig. 1, for $\beta = 0.4$ the model shows puffs, puff splitting, and slugs remarkably like those from full DNS. The model parameter R nearly corresponds to Reynolds number Re .

While positive β is ultimately of interest, to better connect the two models consider first β negative, e.g. $\beta = -0.4$. A transition from puffs to slugs occurs as R increases and the wedge of chaos crosses the u -nullcline. One finds a noisy version of the continuous model in Fig. 2. (See the Appendix Fig. 8.) If splittings of turbulent patches occur, they are exceedingly rare. At $\beta \approx 0$, (including even $\beta = -0.1$), chaotic fluctuations in q cause occasional splitting of expanding turbulence. Puffs at lower R are clearly metastable, persisting for

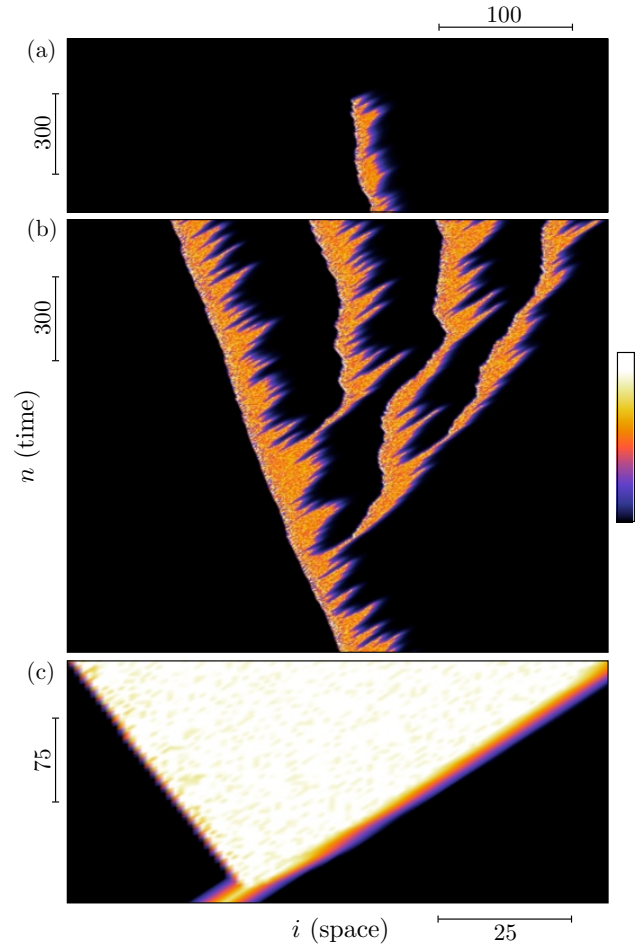


FIG. 4. (Color online) Three regimes of pipe flow from simulations of the discrete model (3)-(6). Space-time diagrams (time upward) illustrate (a) decaying puff at $R = 1900$, (b) puff splitting at $R = 2200$, and (c) slug formation from an edge state at $R = 3000$. For ease of comparison with published work on pipe flow, solutions are shown in a frame co-moving with structures. Turbulence intensity q is plotted with $q = 1.8$ in white. In (a) and (b) the scale is linear with $q = 0$ in black, while in (c) the scale is logarithmic with $q \leq 10^{-3}$ in black. Dimension bars indicate space and time scales. The top space scale applies also to (b).

long times before decaying. However, splitting and decay are unrealistically infrequent if β is too small. Setting $\beta \gtrsim 0.1$ gives realistic behavior, as seen in Fig. 1 where $\beta = 0.4$. (See also the Appendix Fig. 9.) Note that the splitting of expanding turbulent patches and the decay of localized puffs are caused by the same process – the collective escape from the chaotic region of a sufficiently large streamwise interval to bring about local relaminarization. This is precisely the scenario described by extreme fluctuations [33]. In the case of puffs, this results in puff decay, while in the case of splitting, laminar gaps open whose sizes are then set by the recovery of the slow u field.

Figure 4 further illustrates how well the discrete model captures the three regimes of transitional pipe flow. Space-time plots show puff decay, puff splitting, and slug flow. In

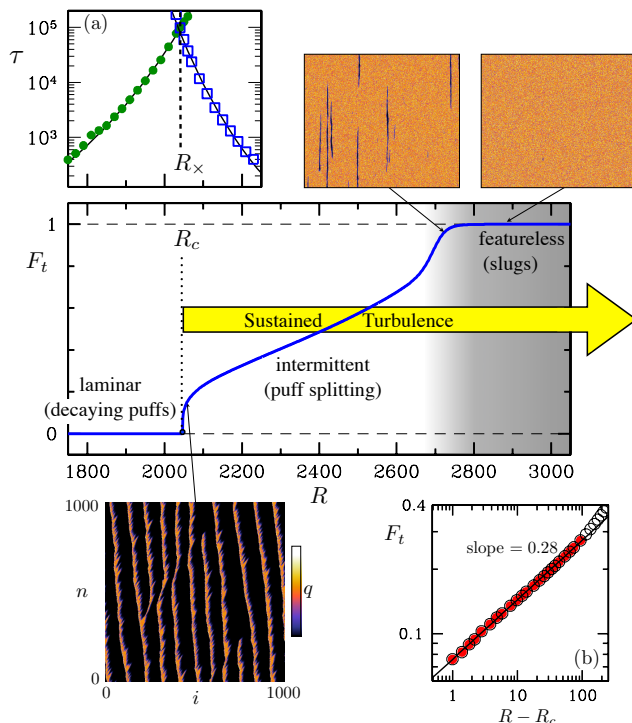


FIG. 5. (Color online) Main figure is a bifurcation diagram for model turbulence in the thermodynamic limit. The turbulence fraction F_t is plotted throughout the transitional regime. The onset of sustained turbulence, via spatiotemporal intermittency, occurs continuously at $R_c \simeq 2046.2$. F_t increases with R and saturates near $R = 2800$. Asymptotic regimes (laminar, intermittent, featureless) are labeled, along with corresponding transient dynamics (decaying puffs, puff splitting, slugs). The onset of featureless turbulence is not sharp as indicated by gray shading. Space-time plots illustrate the dynamics near the ends of the transitional regime ($R = 2058$, $R = 2720$, $R = 2880$) with q plotted in frames co-moving with structures (color map indicated, dark is laminar). (a) Mean lifetimes for decaying (circles) and splitting (squares) puffs crossing at $R_\times \simeq 2040$. (b) log-log plot of F_t versus $R - R_c$. Best fit to the filled (red) points determines R_c and the slope.

Fig. 4(a), a puff persists for only a finite time before abruptly decaying [8–15]. In Fig. 4(b), puff splitting dominates the dynamics [7, 16, 17, 19]. New puffs are generated downstream from existing ones such that intermittent turbulent regions fill space. Compare especially with Refs. 7 and 19. Finally, in Fig. 4(c), a slug arises from a localized edge state (a low-amplitude state on the boundary separating initial conditions which evolve to turbulence from those which decay to laminar flow [18, 34–36]). Compare especially with Ref. 18.

The remainder of the paper provides a global perspective of the transitional regime, obtained from extensive numerical simulation of Eqs. (3)-(4) and summarized in Fig. 5. Turbulence fraction F_t serves as the order parameter, tracking the dynamics from the onset of intermittency through the approach to uniform, featureless turbulence. A point is defined to be turbulent if $q > 0.5\alpha$ and F_t is the mean fraction of turbulent points.

There is a continuous transition to sustained turbulence, via spatiotemporal intermittency [19–24], at a critical value $R_c \simeq 2046.2$. Below R_c , the flow is asymptotically laminar and $F_t = 0$. Above R_c turbulence persists indefinitely and $F_t > 0$. This transition is associated with the crossing of mean lifetimes for puff decay and splitting shown in Fig. 5(a). Both decay and splitting are memoryless processes with exponential survival distributions $P \sim \exp(-n/\tau(R))$, where $\tau(R)$ is the R -dependent mean time until decay or split. (See the Appendix Sec. 2 a and Fig. 12.) The mean lifetimes vary approximately super-exponentially with R [13, 14, 19], but neither is exactly of this form. Mean lifetimes cross at $R_\times \simeq 2040$. Above R_\times an isolated puff is more likely to split than decay. As expected, even though individual turbulent domains may still decay, others may split, as seen in the spacetime plot at $R = 2058$. Due to correlations between splitting and decay events, the critical value R_c is not identical to R_\times , but is very close to it (a difference of 0.3%). Fig. 5(b) shows that just above criticality, $F_t \sim (R - R_c)^{0.28}$, supporting that the transition falls into the universality class of directed percolation [37].

The ratio of turbulence to laminar flow increases through the intermittent region and at the upper end only small laminar flashes are seen within a turbulent background. Beyond $R \simeq 2800$ laminar regions essentially disappear and $F_t \simeq 1$. This occurs in pipe flow at $Re \simeq 2600$ [7]. The transition to featureless turbulence is not sharp, however, nor is the transition from puff splitting to slugs. This upper transition will be addressed elsewhere, but the basic effect, common for bistable media, is already contained in Eqs. (1)-(2). For a range of r above the slug transition, ($r_c < r \lesssim 0.91$), turbulence does not expand to fill the domain in the presence of other slugs. Small laminar regions remain due to the recovery of the slow u -field and this sets the scale for the laminar flashes at the upper end of the transition region in Fig. 5.

I have sought to understand key elements of transitional pipe flow – puffs, puff splitting, and slugs – without appealing in detail to the underlying structures within shear turbulence. This approach is similar to that expounded by Pomeau [20], and considered elsewhere [23]. The important insight here is the close connection between subcritical shear flows and excitable systems. The view is that a great many features of intermittent pipe flow can be understood as a generic consequence of the transition from excitability to bistability where the turbulent branch is itself locally a chaotic repeller. I have introduced particular model equations to express these ideas in simple form. While phenomena have been demonstrated with specific parameters, the phenomena are robust. The challenge for future work is to obtain more quantitatively accurate models, perhaps utilizing full simulations of pipe flow, since ultimately the fluid mechanics of shear turbulence (streaks and streamwise vortices) is important for the details of the process. More challenging is to extend this effort to other subcritical shear flows, such as a plane channel, plane Couette, and boundary-layer flows. These require non-trivial extensions of the current work because, unlike here, the mean shear profile cannot obviously be well captured by a simple scalar field.

ACKNOWLEDGMENTS

I thank M. Avila, Y. Duguet, B. Hof, P. Manneville, D. Moxey, and L. Tuckerman for valuable discussions. Computing resources were provided by IDRIS (grant 2010-1119).

Appendix: Supplemental Information

1. Parameters Selection

Here the parameter selection used in this study is discussed. No attempt has been made to determine precisely values such for the best fit to pipe flow. The models are not sufficiently quantitative that exact comparisons are called for at this time. Moreover, the phenomena presented in the paper are very robust and for some parameters there simply is not a strong criterion to use to select precise values. The goal is to provide justification for the values used in the paper as well as insight into how the parameters control the dynamics of the models.

a. Parameters for continuous model

Only the two rates ϵ_1 and ϵ_2 need to be determined. The value of δ has little impact on the dynamics and has simply been fixed at 0.1. These parameters are determined by fitting to a typical puff from DNS as shown in Fig. 6.

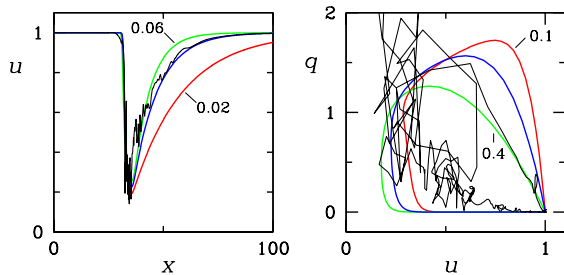


FIG. 6. (Color online) Parameters ϵ_1 and ϵ_2 chosen to match a typical puff from DNS at $Re = 2000$. In the left plot $\epsilon_2 = 0.2$ while ϵ_1 has values 0.02 (red), 0.04 (blue), and 0.06 (green). In the right plot $\epsilon_1 = 0.04$ and ϵ_2 has values 0.1 (red), 0.2 (blue), and 0.4 (green). $r = 0.7$. DNS is the irregular black curve. The unlabeled (blue) curves in the two plots correspond to the values of ϵ_1 and ϵ_2 used in the paper.

The left plot shows the spatial profile of model puffs for three values of ϵ_1 , the parameter controlling the final relaxation to parabolic flow. It is straightforward to select a reasonable value of ϵ_1 from such a plot. Note, however, that a scaling of model length scale has been performed to plot model and DNS profiles on the same graph (model lengths have been multiplied by 0.225). This scaling of length is such that the sharp upstream edge of the model puff occurs over the same distance as in DNS. The upstream edge is largely set by ϵ_2 . (If the scaling of space units between model and DNS were

known for other reasons, then the spatial profile alone could be used to determine both ϵ_1 and ϵ_2 .)

The right plot is used then to complete the determination. Here model puffs for different values of ϵ_2 are plotted in the u - q plane. The sharp upstream edge of a puff is the trajectory rising from parabolic flow at $u = 1, q = 0$ and this is strongly affected by the value of ϵ_2 . If ϵ_2 is too small then the trajectory is too steep (u does not respond quickly enough). If ϵ_2 is too large, then q does not reach a sufficiently large value.

The values of $\epsilon_1 = 0.04$ and $\epsilon_2 = 0.2$ chosen for the simulations presented in the paper were arrived at by varying the two values to get the best overall agreement in the spatial profile and phase portrait.

b. Parameters for discrete model

As stated in the paper, the two rates ϵ_1 and ϵ_2 are taken to have the same values as in the continuous model. This is quite reasonable given the relationship between Eqs. (2) and (4). This leaves choosing the parameters k , β , and γ of the map F , and the parameters c and d . The role of each of these is discussed below. As each parameter is varied in the following, the remaining parameters take the fixed values used in the paper: $\epsilon_1 = 0.04$, $\epsilon_2 = 0.2$, $k = 2$, $\beta = 0.4$, $\gamma = 0.95$, $c = 0.45$, and $d = 0.15$.

Parameter k : The parameter k effectively dictates how many iterates of the map f are used per time step of the model. The effect of the parameter k is shown in Fig. 7 where puff solutions are shown in the u - q phase plane for $k = 1$ and $k = 2$. Model turbulence is more erratic for $k = 2$ than $k = 1$. When $k = 1$, puff splitting and the transition to sustained turbulence occurs at a smaller value of R , but the fact that R is smaller on the top row of Fig. 7 only partially accounts for the difference between the top and bottom rows of Fig. 7.

In addition to this visual comparison, there is the fact that the average slope for a unimodal map with stable chaos is limited to $\lambda = 2$ and this is an artificial constraint on the dynamics that comes about from considering one-dimensional dynamics. (In the case of transient chaos the mean slope can exceed 2, but there is still a constraint relating the escape rate to the mean slope.) Taking $k > 1$ is equivalent to considering multimodal maps and removes the artificial constraint.

Note that the model shows puffs, puff splitting and slugs even for $k = 1$. These features are robust. However, the additional freedom in the chaotic dynamics by allowing $k = 2$ permits the model to achieve a better representation of turbulent flow. I have not found that using $k > 2$ offers noticeable further improvement.

Parameter β : This parameter controls the leakage rate from the chaotic region of the map. Figure 8 shows examples of states for $\beta = -0.4$ and $\beta = 0$. With β sufficiently negative, as for $\beta = -0.4$ in the top row of Fig. 8, a transition from puffs to slugs occurs that is essentially just a noisy version of the continuous models shown in Fig. 2 of the paper. Note that the chaotic wedge first touches the u -nullcline at $R = 1733$ and the transition from puffs to slugs occurs near to, but not exactly at, this value. If there are any splitting events they are

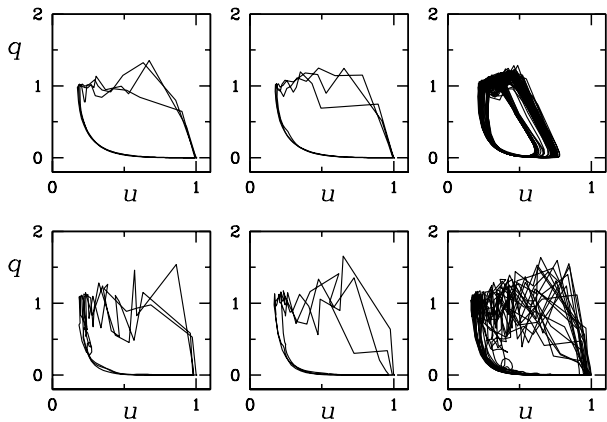


FIG. 7. Effect of parameter k . Top row $k = 1$ and bottom row $k = 2$. In each case snapshots are plotted in the u - q phase plane. The left two plots show randomly chosen snapshots of solutions with three closely spaced puffs. The right-most plots are of solutions following a quench from high R and contain a large number of puffs. Top row is at $R = 1760$ and the bottom row is at $R = 2000$. Both values of R are close to the transition to sustained turbulence for the corresponding value of k .

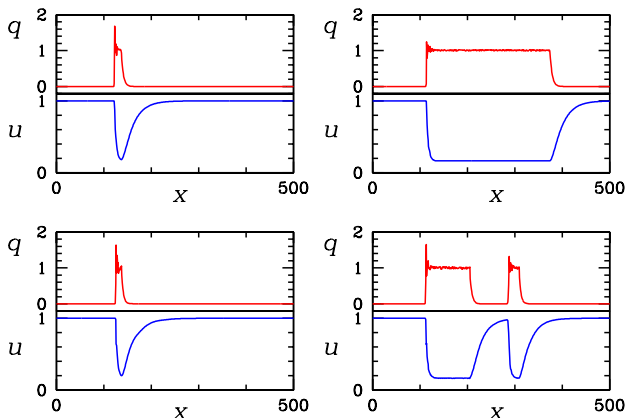


FIG. 8. (color online) Effect of parameter β . Top row $\beta = -0.4$ and bottom row $\beta = 0$. In each case snapshots of solutions are shown on either side on the transition from localized puffs to expanding turbulence. Upper left: $R = 1750$. Upper right: $R = 1780$. Lower left: $R = 1760$. Lower right: $R = 1800$.

very rare.

With $\beta \approx 0$, as for $\beta = 0$ in the bottom row of Fig. 8, the transition from puffs to slugs is mediated by splitting events. However, the splitting events are too rare for the model to realistically correspond to pipe flow.

As illustrated in Fig. 9, with $\beta \gtrsim 0.1$, model puff splitting is similar to pipe flow. There appears to be no strong basis to select any particular value of β based on a visual examination of the onset of splitting. The value $\beta = 0.4$ used in the paper is simply a representative value.

Parameter γ : This parameter controls the monotone decay of turbulence q following exit from the chaotic region. Figure 10 shows puffs plotted in the u - q phase plane for two value

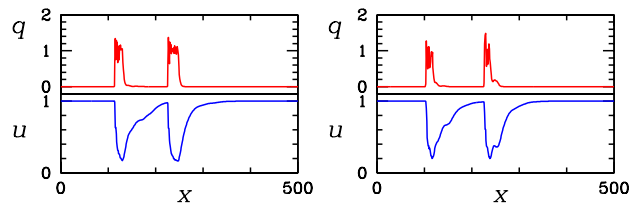


FIG. 9. (color online) Further effect of parameter β . Left $\beta = 0.3$ ($R = 1980$) and right $\beta = 0.5$ ($R = 2180$). In each case snapshots of solutions are shown just after a puff split. There is little to distinguish the cases.

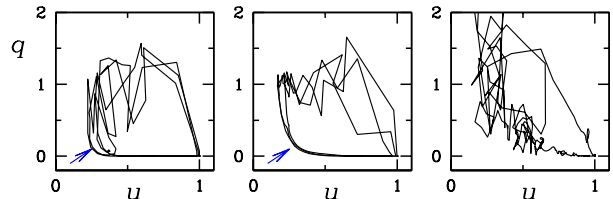


FIG. 10. (Color online) Effect of parameter γ . Left shows $\gamma = 0.80$, with $R = 2400$, middle shows $\gamma = 0.95$, with $R = 2000$, and is the same plot as bottom middle of Fig. 2. Arrows indicate the relevant region of the u - q phase plane. The right-most plot is DNS of a puff at $Re = 2000$, exactly the same as in Fig. 1.

of γ . For comparison the puff at $Re = 2000$ from Fig. 6 is repeated here. The smaller γ , the more quickly q decays and the less rounded the phase-space dynamics is in the lower left corner of the phase portraits. The best match of turbulent decay in the model will be at the largest possible value for γ . However, as γ approaches 1 laminar flow becomes marginally stable to q perturbations and this is clearly unphysical. The value $\gamma = 0.95$ was chosen as a compromise between the competing requirements of having γ large but not too close to 1. An improvement could be likely be obtained by having γ be a function of u and R , but this introduces additional fitting parameters and is not done here.

Parameters c and d : These parameters are naturally thought of as arising from the discretization of the terms u_x and q_{xx} in the continuous model. At present I am not aware of any compelling reasons to select c and d to particular values other than that they should be small (d must satisfy $d \lesssim 1/2$ for stability reasons). The value of c was chosen to be less slightly less than $1/2$. The value of d is then to be fixed. Based on the analogy with the continuous model, and the value chosen for c , it could be taken to be $d = c^2$. This is because discretizing the continuous model with a time step of $\Delta t = 1$ means that $c = 1/\Delta x$, from an upwind discretization of the advection term. Then d will be $1/(\Delta x)^2$ from discretization of the diffusion term. This would give $d = 0.45^2 = 0.2025$. However, adjusting d downwards from this value to $d = 0.15$ places the transition to sustained turbulence in the model at the critical Reynolds number for pipe flow. Having the model match this transition point seems preferable to setting it to the particular value 0.2025. Moreover, it is common to vary the diffusive coupling constant in studies of coupled-map lattices.

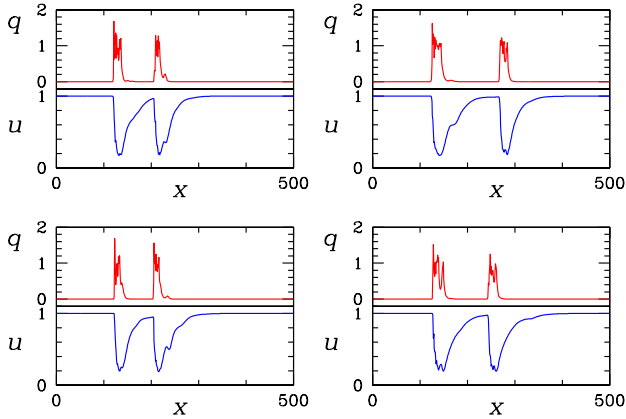


FIG. 11. (Color online) Effect of parameters c and d . In each case snapshots of solutions are shown just after a puff splitting. Splitting is not very sensitive to c and d around values used in the paper. Upper left: $c = 0.45$, $d = 0.1$, $R = 2480$. Upper right: $c = 0.45$, $d = 0.2025$, $R = 1960$. Lower left: $c = 0.35$, $d = 0.15$, $R = 2120$. Lower right: $c = 0.55$, $d = 0.15$, $R = 2080$.

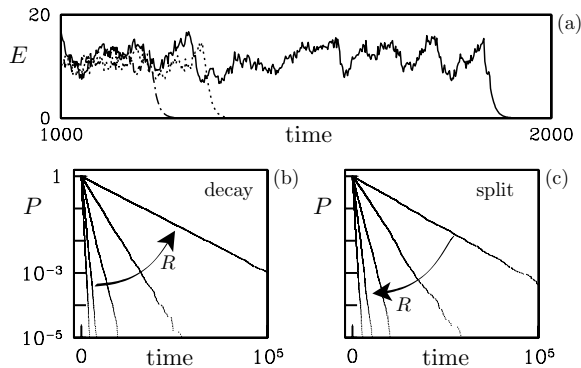


FIG. 12. Lifetime statistics for decaying and splitting model puffs. (a) Time series of total energy E for three puffs illustrating abrupt decay at unpredictable times ($R = 1800$). Bottom row shows exponential (memoryless) probabilities P for (b) decaying puffs ($R = 1800, 1850, 1900, 1950, 2000$) and (c) splitting puffs ($R = 2060, 2090, 2120, 2150, 2180$).

To emphasize that qualitative features of the model do not strongly depend on the parameters c and d (as long as they are reasonably small), Fig. 11 shows some splitting puffs for different values of c and d . The reason for focusing on splitting puffs is these best show the fidelity of the model. Puffs and slugs are easily obtained. In each case a puff was generated and R was increased slowly until a splitting occurred.

The value of R are given in the caption.

2. Details of Numerical Study in Figure 4

a. Decay and Splitting Statistics

Figure 12(a) shows time series of total energy $E = \sum_i q_i$ for puffs from three initial conditions in which q is varied at one space point by less than 10^{-5} . While the dynamics are deterministic, abrupt decay occurs at unpredictable times. From a large number of such simulations lifetime statistics can be generated. Specifically, simulations were initiated from small perturbations designed to trigger puffs. A random number generator was used to introduce a small amount of randomness into each perturbation. Simulations were then run for 1000 time steps to allow puffs to equilibrate. If puffs had not decayed, the puffs were used as initial conditions for simulations for decay statistics. Figure 12(b) shows representative survival probabilities P of a puff lasting at least time n . Each distribution corresponds to 4000 realizations. The survival functions are exponential (memoryless), $P \sim \exp(-n/\tau(R))$, where $\tau(R)$ is the R -dependent mean lifetime until decay.

Puff splitting is similar. Initial conditions were generated in the same way only here equilibration simulations were run for 1400 time steps because at the largest R in the study 1000 time steps was not quite enough to remove all equilibration effects. A puff was defined to have split once two turbulent peaks are separated by least 80 grid points. Figure 12(c) shows representative survival probabilities P for a puff to last at least time n without splitting. The distributions are again exponential, $P \sim \exp(-n/\tau(R))$, showing that model splitting is indeed memoryless with a mean splitting time $\tau(R)$. These lifetimes are plotted in Fig. 4(a) of the paper.

b. Turbulence Fraction

The turbulence fraction F_t serves as the order parameter for the onset of sustained turbulence. A point is defined to be turbulent if $q > \kappa\alpha$ where κ sets a threshold relative to the lower boundary separating chaotic and monotonic decay of the map F . F_t is the mean fraction of grid points in the turbulent state. Means have been computed from 4 independent simulations. For R near the critical point, simulations of 8×10^6 time steps were run on grids of 12×10^4 points. The standard deviation from the 4 independent simulations is comparable to the point size in Fig. 4(b) of the paper. For $R > 2200$ simulations for 10^6 time steps on grids of 10^4 points were more than sufficient. In Fig. 4 of the paper, F_t is plotted for $\kappa = 0.5$. While the exact value of F_t depends on threshold κ , the extent of the intermittent region and critical scaling at onset do not.

[1] O. Reynolds, Phil. Trans. R. Soc. Lond. A **174**, 935 (1883).
[2] A. Darbyshire and T. Mullin, J. Fluid Mech. **289**, 83 (1995).

[3] B. Hof, A. Juel, and T. Mullin, Phys. Rev. Lett. **91**, 244502 (2003).

[4] J. Peixinho and T. Mullin, J. Fluid Mech. **582**, 169 (2007).

- [5] J. Rotta, *Ing-Arch.* **24**, 258 (1956).
- [6] I. Wygnanski and H. Champagne, *J. Fluid Mech.* **59**, 281 (1973).
- [7] D. Moxey and D. Barkley, *Proc. Nat. Acad. Sci.* **107**, 8091 (2010).
- [8] H. Faisst and B. Eckhardt, *J. Fluid Mech.* **504**, 343 (2004).
- [9] J. Peixinho and T. Mullin, *Phys. Rev. Lett.* **96**, 094501 (2006).
- [10] B. Hof, J. Westerweel, T. M. Schneider, and B. Eckhardt, *Nature* **443**, 59 (2006).
- [11] A. P. Willis and R. R. Kerswell, *Phys. Rev. Lett.* **98**, 014501 (2007).
- [12] T. M. Schneider and B. Eckhardt, *Phys. Rev. E* **78**, 046310 (2008).
- [13] B. Hof, A. de Lozar, D. Kuik, and J. Westerweel, *Phys. Rev. Lett.* **101**, 214501 (2008).
- [14] M. Avila, A. P. Willis, and B. Hof, *J. Fluid Mech.* **646**, 127 (2010).
- [15] D. J. Kuik, C. Poelma, and J. Westerweel, *J. Fluid Mech.* **645**, 529 (2010).
- [16] I. Wygnanski, M. Sokolov, and D. Friedman, *J. Fluid Mech.* **69**, 283 (1975).
- [17] M. Nishi, B. Ünsal, F. Durst, and G. Biswas, *J. Fluid Mech.* **614**, 425 (2008).
- [18] Y. Duguet, A. P. Willis, and R. R. Kerswell, *J. Fluid Mech.* **663**, 180 (2010).
- [19] K. Avila, D. Moxey, A. de Lozar, M. Avila, D. Barkley, and B. Hof, (to be published).
- [20] Y. Pomeau, *Physica D* **23**, 3 (1986).
- [21] H. Chaté and P. Manneville, *Physica D* **32**, 409 (1988).
- [22] H. Chaté and P. Manneville, *Europhys Lett* **6**, 591 (1988).
- [23] S. Bottin and H. Chaté, *Eur Phys J B* **6**, 143 (1998).
- [24] P. Manneville, *Phys. Rev. E* **79**, 025301 (2009).
- [25] H. Blackburn and S. Sherwin, *J Comput Phys* **197**, 759 (2004).
- [26] B. Hof, A. de Lozar, M. Avila, X. Tu, and T. M. Schneider, *Science* **327**, 1491 (2010).
- [27] R. Narasimha and K. Sreenivasan, *Advances in applied mechanics* **19**, 221 (1979).
- [28] J. Tyson and J. Keener, *Physica D* **32**, 327 (1988).
- [29] J. Keener and J. Sneyd, *Mathematical Physiology I: Cellular Physiology*, 2nd ed. (Springer, New York, 2008).
- [30] A. Hodgkin and A. Huxley, *J Physiol-London* **117**, 500 (1952).
- [31] B. Eckhardt, T. M. Schneider, B. Hof, and J. Westerweel, *Annu. Rev. Fluid Mech.* **39**, 447 (2007).
- [32] J. Vollmer, T. M. Schneider, and B. Eckhardt, *New J Phys* **11**, 013040 (2009).
- [33] N. Goldenfeld, N. Guttenberg, and G. Gioia, *Phys. Rev. E* **81**, 035304 (2010).
- [34] T. Schneider, B. Eckhardt, and J. Yorke, *Phys. Rev. Lett.* **99**, 034502 (2007).
- [35] T. M. Schneider and B. Eckhardt, *Phil. Trans. R. Soc. A* **367**, 577 (2009).
- [36] F. Mellibovsky, A. Meseguer, T. M. Schneider, and B. Eckhardt, *Phys. Rev. Lett.* **103**, 054502 (2009).
- [37] H. Hinrichsen, *Adv. Phys.* **49**, 815 (2000).